

## Muon Polarization in $K_{\mu 3}^0$ -Meson Decay\*

R. J. ABRAMS,\*\*† A. ABASHIAN, R. E. MISCHKE,† B. M. K. NEFKENS,§  
 J. H. SMITH, R. C. THATCHER,|| L. J. VERHEY,§ and A. WATTENBERG  
 Department of Physics, University of Illinois, Urbana, Illinois 61801  
 (Received 13 August 1968)

The polarization of the muon in the decay  $K_L^0 \rightarrow \pi^- \mu^+ \nu$  was measured in a spark-chamber experiment. For the decay phase space measured in this experiment, the results are  $\alpha \bar{P}_L = 0.31 \pm 0.07$ ,  $\alpha \bar{P}_T = -0.02 \pm 0.07$ , and  $\alpha \bar{P}_P = -0.10 \pm 0.07$ , where  $\bar{P}_L$ ,  $\bar{P}_T$ , and  $\bar{P}_P$  are the average components of polarization along the muon momentum, transverse to the decay plane, and perpendicular to the muon in the decay plane. The analyzing parameter  $\alpha$  of the muon decay is about 0.35 in this experiment. From the above polarization results, assuming energy-independent form factors, we obtain the ratio of form factors  $\xi = f_-/f_+$ ; the results are  $\text{Re}\xi = -1.6 \pm 0.5$  and  $\text{Im}\xi = -0.2 \pm 0.6$ .

### I. INTRODUCTION

AN experiment was undertaken to measure the muon polarization in the decay  $K_L^0 \rightarrow \pi^- + \mu^+ + \nu$ . A measurement of the total polarization of the muon yields two pieces of information that are of importance in the study of weak interactions. First, the existence of a nonzero component of polarization transverse to the decay plane would indicate a violation of time-reversal invariance. Second, the components of polarization within the decay plane are sensitive functions of the form factors, the parameters that appear in theoretical analysis of  $K$ -meson decays. Consequently, the polarization can yield specific detailed information on the weak interaction involved in the  $K$ -meson decay process.

The matrix element is of the form

$$M \sim [(p_K + p_\pi)_\lambda f_+(q^2) + (p_K - p_\pi)_\lambda f_-(q^2)] \times [\bar{\mu} \gamma_\lambda (1 + \gamma_5) \nu], \quad (1)$$

where  $p_K$  and  $p_\pi$  are the four-momenta of the  $K$  meson and  $\pi$  meson, respectively;  $f_+(q^2)$  and  $f_-(q^2)$  are two form factors that specify the behavior of the hadron current;  $q$  is the momentum transfer between the  $K$  meson and the  $\pi$  meson.  $\bar{\mu}$  and  $\nu$  represent the wave functions of the lepton and neutrino, respectively.  $\gamma_\lambda$  and  $\gamma_5$  are Dirac matrices. The above matrix element is in the form of a product of a hadron current and a lepton current with a vector interaction.

The polarization of the muon in  $K_{\mu 3}$  decay has been calculated by several authors.<sup>1</sup> We will use the result as

derived by Cabibbo and Maksymowicz. The polarization is computed in the muon rest frame. The result is expressed in terms of the momenta in the  $K$  rest frame. The polarization vector is  $\mathbf{P} = \mathbf{A}/|\mathbf{A}|$ , where

$$\mathbf{A} = a_1(\xi) \mathbf{p}_\mu - a_2(\xi) \{ \mathbf{p}_\mu [(M_K - E_\pi)/m_\mu + (\mathbf{p}_\pi \cdot \mathbf{p}_\mu)(E_\mu - m_\mu)/m_\mu |\mathbf{p}_\mu|^2] + \mathbf{p}_\pi \} + M_K \text{Im}\xi(q^2) (\mathbf{p}_\pi \times \mathbf{p}_\mu), \quad (2)$$

and

$$\begin{aligned} \xi(q^2) &= f_-(q^2)/f_+(q^2), \\ a_1(\xi) &= 2M_K^2 [E_\nu + \text{Re}b(q^2)(E_\pi^* - E_\pi)]/m_\mu, \\ a_2(\xi) &= M_K^2 + 2 \text{Re}b(q^2)M_K E_\mu + |b(q^2)|^2 m_\mu^2, \\ b(q^2) &= \frac{1}{2} [\xi(q^2) - 1], \\ E_\pi^* &= (M_K^2 + m_\pi^2 - m_\mu^2)/2M_K. \end{aligned}$$

$a_1(\xi)$  and  $a_2(\xi)$  are scalar functions which depend on the real part of the form factor ratio  $\xi(q^2)$ .

The last term in Eq. (2) is the component of polarization transverse to the decay plane. Several groups have previously reported<sup>2</sup> that this component was zero within the experimental error. That result is in agreement with time-reversal invariance.

The other two components of the polarization are in the decay plane; it is convenient to take one component  $P_L$  along the muon momentum and the other component  $P_P$  perpendicular to the muon momentum. The value of the ratio of the form factors  $f_-/f_+ = \xi$  has a strong dependence on  $P_P/P_L$ , which is the tangent of the angle of the polarization vector relative to the momentum of the muon. As can be seen from Eq. (2), the dependence is a function of the portion of the Dalitz plot being measured.

We obtain an average value for  $\xi$  over the entire Dalitz plot, by measuring average values of  $\bar{P}_L$  and  $\bar{P}_P$ . We have also evaluated  $P_L$  and  $P_P$  for two halves of the Dalitz plot to check for a possible energy dependence of  $\xi$ . The statistical accuracy was inadequate for any conclusion to be drawn about the energy dependence.

\* Work supported in part by the U. S. Atomic Energy Commission.

\*\* This work is based on a thesis submitted by R. J. Abrams in partial fulfillment of the requirements for the Ph.D. degree in Physics at the University of Illinois, Urbana, Ill.

† Present address: Brookhaven National Laboratory, Upton, N. Y.

‡ Present address: Princeton University, Princeton, N. J.

§ Present address: University of California at Los Angeles, Los Angeles, Calif.

|| Present address: Carnegie-Mellon University, Pittsburgh, Pa.

<sup>1</sup> J. J. Sakurai, Phys. Rev. **109**, 980 (1958); S. W. MacDowell, Nuovo Cimento **9**, 258 (1958); J. Nilsson, Nucl. Phys. **14**, 639 (1960); N. Cabibbo and A. Maksymowicz, Phys. Letters **9**, 352 (1964); **11**, 213(E) (1964); **14**, 72(E) (1965).

<sup>2</sup> D. Bartlett, C. E. Friedberg, K. Goulianos, and D. Hutchinson, Phys. Rev. Letters **16**, 282 (1966); R. J. Abrams, A. Abashian, R. E. Mischke, B. M. K. Nefkens, J. H. Smith, R. C. Thatcher, L. J. Verhey, and A. Wattenberg, *ibid.* **17**, 606 (1966); K. K. Young, M. J. Longo, and J. A. Helland, *ibid.* **18**, 806 (1967).

The perpendicular polarization in  $K_{\mu 3}^0$  decay has also been measured by Auerbach *et al.*,<sup>3</sup> who obtain a value for the perpendicular polarization of  $P_P = -0.28 \pm 0.12$  and  $\xi = -1.2 \pm 0.5$ . Other experiments which give values of  $\xi$  have been summarized by Auerbach *et al.*<sup>4</sup> and by Lee and Wu.<sup>5</sup>

## II. EXPERIMENTAL ARRANGEMENT

### A. Beam Layout

The experiment was performed in a neutral beam at the Argonne National Laboratory Zero Gradient Synchrotron (ZGS). The ZGS proton beam impinged on a beryllium target ( $\frac{1}{4}$  in. thick  $\times \frac{1}{4}$  in.  $\times \frac{1}{8}$  in.) which was located in the  $L3$  straight section (see Fig. 1). A set of four collimators ( $CL1$ ,  $CL2$ ,  $CL3$ , and  $CL4$ ) were positioned along a straight line at  $31^\circ$  to the proton direction.  $\gamma$  rays were attenuated by a 2-in.-thick lead brick placed in the beam ahead of the first collimator  $CL1$ . Charged particles were swept out of the beam by a magnet located between  $CL2$  and  $CL3$ . The upstream end of  $CL4$ , located 45.5 ft from the target, was the defining aperture. This aperture, 1.2 in.  $\times$  1.8 in., subtended a solid angle of  $7.2 \times 10^{-6}$  sr. The experimental apparatus was set up about 55 ft from the target.

### B. Apparatus

The experimental arrangement is shown in Fig. 2. The fiducial volume for the  $K_L^0$  decays was within a vacuum pipe that had Mylar side windows 0.003 in. thick. Tracks of the charged decay products were

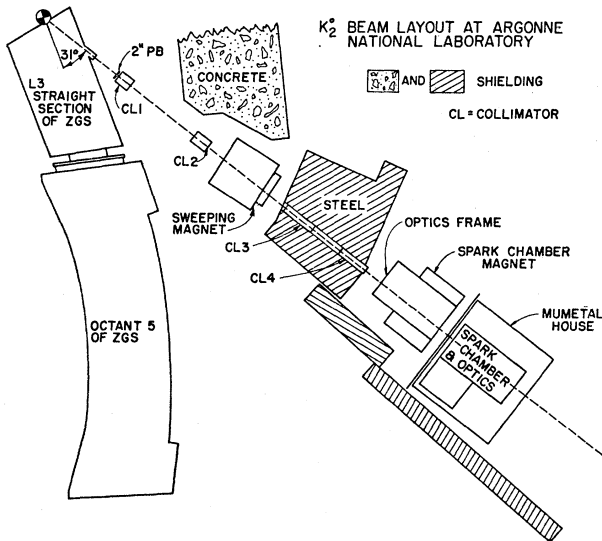


FIG. 1. Neutral beam layout at Argonne ZGS.

<sup>3</sup> L. B. Auerbach, A. K. Mann, W. K. McFarlane, and F. J. Sciulli, *Phys. Rev. Letters* **17**, 980 (1966).

<sup>4</sup> L. B. Auerbach, A. K. Mann, W. K. McFarlane, and F. J. Sciulli, *Phys. Rev. Letters* **19**, 464 (1967).

<sup>5</sup> T. D. Lee and C. S. Wu, *Ann. Rev. Nucl. Sci.* **16**, 471 (1966).

recorded in the momentum spark chambers. The momentum spark chambers were situated in a magnetic field. An absorber consisting of 2.9 collision lengths of material (4 in. of brass and 20 in. of aluminum) was installed in the yoke of the magnet immediately downstream from the momentum spark chambers. The absorber was used to remove or scatter pions by nuclear interaction. The muons in which we were interested passed through the absorber without nuclear interactions and entered the range spark chambers.

An idealized decay  $K_L^0 \rightarrow \pi^- + \mu^+ + \nu$  is sketched in Fig. 2 with the decay occurring in the vacuum pipe. The  $\pi^-$  and  $\mu^+$  tracks are seen in the momentum spark chambers. The  $\pi^-$  meson disappears in the absorber, while the  $\mu^+$  goes through the absorber, stops, and decays ( $\mu^+ \rightarrow e^+ + \nu + \bar{\nu}$ ) in the so-called "range chambers."

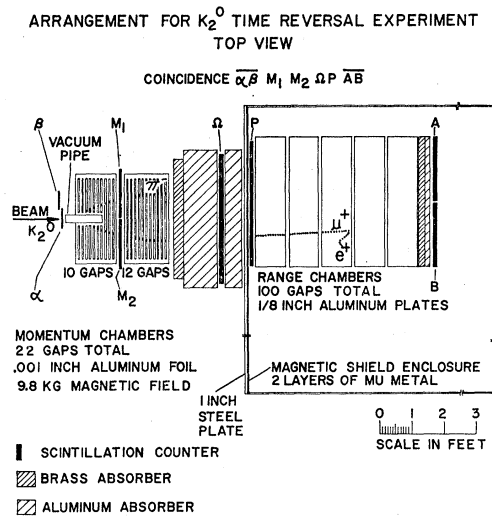
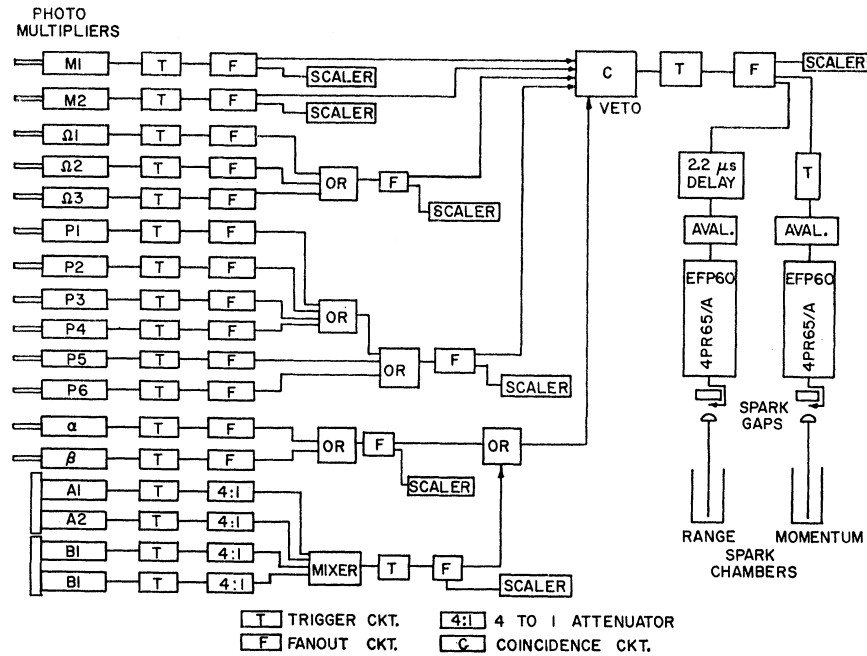


FIG. 2. Experimental apparatus plan.

The range spark chambers consisted of five identical units, each having 20 gaps. All plates were  $\frac{1}{8}$ -in.-thick aluminum, 36 in. high  $\times$  48 in. wide. Muons in the momentum interval from 540 to 750 MeV/ $c$  passed through the absorber and stopped in the range chambers. To minimize the precession of the muons that stopped in the range chambers, a "mu-metal" magnetic shield house was built around the range chambers. The average magnetic field at the range chambers inside the house was about 0.3 G. Without the shield house the field was about a factor of 10 higher.

The spark chambers were photographed with four Beattie-Coleman 35-mm cameras that were modified to use Schneider Super-Angulon lenses. The momentum spark chambers were photographed with one camera; approximately  $90^\circ$  stereo was obtained using a mirror inside the magnet. The range spark chambers were photographed with three cameras. Two cameras viewed the chambers from the top, one from the side.

Fig. 3. Electronics block diagram.



### C. Triggering and Electronics

The scintillation counters are indicated in Fig. 2. Counters  $\alpha$  and  $\beta$  were used to veto charged particles which entered the apparatus. Counters  $M1$ ,  $M2$ ,  $\Omega$ , and  $P$  were required to form a fourfold coincidence; the logic is shown in Fig. 3. University of Illinois modular electronics were used. Counters  $A$  and  $B$ , which were employed only 10% of the time, were used to veto muons which went completely through the range chambers. The trigger  $\bar{\alpha}\beta M1M2\Omega P$  that was used mainly ensured that (1) a neutral particle entered the vacuum, (2) two charged particles were produced before the counters in the magnet, (3) a charged particle entered the range chambers. The counters  $\alpha$ ,  $\beta$ ,  $M1$ , and  $M2$  were made of  $\frac{1}{8}$ -in.-thick plastic. To allow a substantial percentage of the stopped muons to decay (about 60%), the range chambers were triggered after a delay of 2.2  $\mu$ sec. A small clearing field of 1 V was used in conjunction with the delayed firing of the range chambers.

### D. Operational Procedures

The field of the magnet was mapped before and after the experiment. All the counters had radioactive standards and these were checked about once a day. The singles and coincidence counting rates, all high voltage, and the magnet shunt current were monitored every 2 or 3 h. Every 1000 pictures a test strip was taken and the efficiencies of the spark chambers were checked. The stray and earth's magnetic field inside the mu-metal house was initially checked on a daily basis with a large flip coil. Later in the experiment this check was made

about once a week. The neutral beam profile and position was checked at the start of every running period by means of a polaroid scintillation camera to determine whether the ZGS target position was correctly set.

## III. DATA REDUCTION AND MEASUREMENTS

### A. Scanning

Two views of the range chambers film were scanned to find events that apparently had a stopped muon accompanied by its decay electron. The signature of such an event was a stopped track that had a kink at its end. The minimum acceptable kink length was four gaps (3.8 g/cm<sup>2</sup> aluminum); the maximum acceptable length was 30 gaps. The minimum acceptable opening angle between the kink and the stopping track was 10°.

Of the 415 000 pictures, 47 000 (11%) were found to have an acceptable stopping track and kink. Some 332 000 of the pictures did not have a track which stopped in the range chambers. Some 36 000 of the pictures had a stopped track but did not have an acceptable kink. Of the 47 000 acceptable pictures, only those 30 000 pictures that had a minimum opening angle of 30° were retained for further analysis. Events in the omitted forward cone contained a contamination from forward scatters and one-prong interactions. The number of different types of events is summarized in Sec. I of Table I.

The 30 000 event candidates were further scanned to determine whether there was a possible  $K_L^0$  decay in the momentum spark chambers. A possible  $K_L^0$  was defined to be two tracks apparently intersecting in the region of the vacuum pipe. Each track was required to have a

TABLE I. Data reduction summary.

Description	Rejected	Accepted
Total number of pictures		415 000
I. Scanning		
A. Range chambers		
1. No stopping track	332 000	
2. Stopping track but no kink $\geq 10^\circ$	36 000	
3. Stopping track but $10^\circ \leq \text{kink} \leq 30^\circ$	17 000	
Sum: Rejected	385 000	- 385 000
Accepted possible muon decays		30 000
B. Momentum chambers		
1. Nonintersecting tracks	6000	
2. Intersection beyond limits	3000	
3. Three-prong interaction	4000	
4. Other	3000	
Sum: Rejected	16 000	- 16 000
Accepted possible $K$ decay plus possible muon decay		14 000
II. Measurement		
A. Fitting		
1. Fitting criteria not satisfied	1000	
2. Both tracks same curvature	500	
3. Helix intersection not good	400	
4. Helix intersection outside fiducial volume	3500	
Sum: Rejected	5400	- 5400
Acceptable fit		8600
B. Kinematics		
1. Failed to satisfy $K_{\mu 3}$ or $K_{e 3}$ kinematics	1600	
2. Satisfied $K_{e 3}$ but not $K_{\mu 3}$ kinematics	1000	
Sum: Rejected	2600	- 2600
Acceptable $K_{\mu 3}$		6000
III. Range-momentum		
Outside limits of $\pm 11\%$	3000	- 3000
Acceptable		3000
IV. Scattering		
Outside limits of 10 in.	1000	- 1000
Good events		2000

minimum of four sparks. A total of 14 000 possible  $K_L^0$  decays were found (43%). The reasons for rejecting pictures were

(1) nonintersecting tracks (6000) which included events in which a track suffered a visible scatter and events with insufficient sparks,

(2) intersection beyond scanning limits (3000) which included two-prong interactions in foils or scintillator,

(3) three-prong interactions in foils or scintillator (4000),

(4) others (3000) which included possible decays or interactions with only one visible track.

A sample of about 25% of the film was rescanned.

The second scan increased the sample by about 5%, indicating a scanning efficiency of about 95%.

## B. Measurement and Computer Processing

The two tracks in the momentum spark chambers were digitized by means of a Hydel measuring machine. Section II of Table I summarizes the various types of events and the reasons for rejecting the unsuccessful ones.

Of the 14 000 measured events, 8600 were successfully reconstructed and fitted. A large number of the measured events (3500) were rejected because the intersection of the helices (decay vertex) occurred outside the fiducial volume of the vacuum pipe. Most of these decays occurred beyond the downstream limit of the fiducial volume. Five hundred were rejected because both tracks had the same curvature, which probably indicated a spurious track or a scatter in one track; an additional 400 of the events failed because the distance of closest approach of the helices was not within the 0.3-in. limit. One thousand were rejected in fitting helices to the sparks. Helix trajectories were corrected to account for the nonuniform magnetic field.

Events that had been successfully fitted (about 8600 events) were further analyzed with kinematics programs similar to those of Carpenter<sup>6</sup> and Fisher.<sup>7</sup> From the laboratory momenta of the two tracks, the center-of-mass energies and momenta were computed with different assumptions for the decay modes of the  $K_L^0$ . Approximately 1600 measured events failed to satisfy either  $K_{\mu 3}^0$  or  $K_{e 3}^0$  kinematics. One thousand events were consistent with  $K_{e 3}^0$  decay but not with  $K_{\mu 3}^0$  decay, and these were also rejected. Six thousand events were kinematically consistent with  $K_{\mu 3}^0$  decay.

## C. Muon Identification Criteria: Scattering and Range-Momentum

The particles that stopped in the range spark chambers passed through a thick absorber which was located between the momentum spark chambers and the range chambers (see Fig. 2). To eliminate pions that had undergone a nuclear scattering in the absorber we rejected any events that had scattered more than approximately two standard deviations from the expected multiple Coulomb scattering for a muon. The scattering in the absorber was determined by comparing the measured position of the track entering the range chambers with its expected position. The expected positions were computed from an extrapolation of both trajectories in the momentum spark chambers. An rms scattering distance of 5.5 in. is expected for a 600-MeV/ $c$  muon passing through the absorber. Events were accepted that entered the range chambers within 10 in. of their expected positions. The sign of the muon

<sup>6</sup> D. W. Carpenter, thesis, University of Illinois, 1965 (unpublished).

<sup>7</sup> G. P. Fisher, thesis, University of Illinois, 1964 (unpublished).

was deduced from the sign of the matching track in the momentum spark chambers.

In addition to the scattering criterion, we employed a range-momentum criterion. The measured momentum of the stopping track was required to be consistent with the expected momentum of a muon that had traversed the same amount of material. A histogram of the fractional deviation of the expected momentum from the measured momentum is shown in Fig. 4. The full width at half-maximum is 7%. The momentum measurement has an accuracy of  $\pm 3\%$ , while the range straggling for 600-MeV/c muons is approximately  $\pm 3\%$ . Events within  $\pm 11\%$  were accepted.

Approximately 1000 candidates were rejected due to the scattering criterion; approximately 3000 were rejected due to the range-momentum tests.

#### D. Range-Chamber Measurements

The range-chamber measurements provided positions and angles of the tracks of the entering muon, the stopping muon and the decay positron. The tracks were hand measured by means of templates and Recordak film readers. All three views were measured. The positron tracks, which often scattered, were measured along the first four sparks, in general. The first three sparks were used if the fourth spark was noticeably out of line.

The measurement accuracy was determined from the reproducibility of repeated measurements and the consistency of the reconstructions using different pairs of views. The accuracy of the reconstructed muon angles was typically about  $2^\circ$ . The positron track angle was typically accurate to about  $7^\circ$ . The uncertainty in this angle results in an error in the final result which is negligible compared to the statistical accuracy.

### IV. DATA ANALYSIS

#### A. Polarization Components and Kinematic Ambiguity

The angular distribution of positrons from the decay of polarized muons is known to be of the form

$$dN_e/d(\cos\theta) = 1 + \alpha \bar{P} \cos\theta, \quad \cos\theta = \hat{P} \cdot \hat{e}, \quad (3)$$

where  $\hat{P}$  and  $\hat{e}$  are unit vectors along the directions of the muon polarization and the positron momentum, respectively. The quantity  $\bar{P}$ , the degree of polarization, is expected to be unity. The parameter  $\alpha$  is the asymmetry parameter of muon decay. For the entire positron spectrum,  $\alpha = 0.33$ . For the portion of the positron spectrum used in this experiment,  $\alpha$  is estimated to be 0.35; there is no experimental evidence of depolarization in aluminum.

It is convenient to consider components of the polarization unit vector  $\hat{P}$  along three orthogonal directions relative to the muon momentum  $\mathbf{p}_\mu$  and pion momentum  $\mathbf{p}_\pi$  in the  $K_L^0$  rest frame:

$$\hat{P} = P_L \hat{u}_L + P_T \hat{u}_T + P_P \hat{u}_P. \quad (4)$$

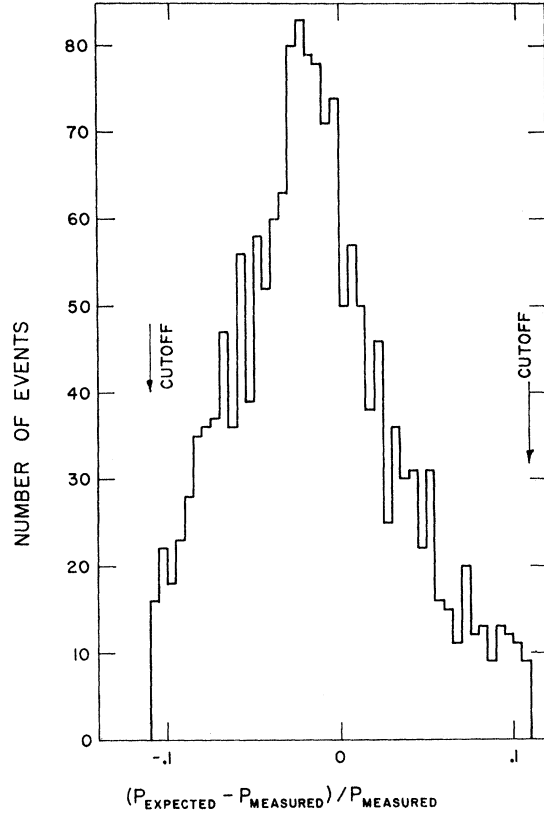


FIG. 4. Fractional deviation of expected momentum based on range for muons compared with measured momentum of particles which stopped in the range spark chambers.

The three directions are

- (1) longitudinal:

$$\hat{u}_L = \mathbf{p}_\mu / |\mathbf{p}_\mu|, \quad (5)$$

- (2) transverse, i.e., normal to the decay plane:

$$\hat{u}_T = (\mathbf{p}_\pi \times \mathbf{p}_\mu) / |\mathbf{p}_\pi \times \mathbf{p}_\mu|, \quad (6)$$

- (3) "in-plane-perpendicular," i.e., perpendicular to the muon momentum within the decay plane:

$$\hat{u}_P = \mathbf{p}_\mu \times (\mathbf{p}_\pi \times \mathbf{p}_\mu) / |\mathbf{p}_\mu \times (\mathbf{p}_\pi \times \mathbf{p}_\mu)|; \quad (7)$$

the three components of polarization  $P_L$ ,  $P_T$ , and  $P_P$  can be obtained from the slopes of the three angular distributions. The analysis is complicated by a twofold ambiguity in the  $K_L^0$  decay kinematics.

The kinematic ambiguity is present because neither the energy of the  $K_L^0$  meson was measured nor the neutrino detected. Two possible values of the  $K_L^0$ -meson energy  $E_K$  result:

$$\frac{E_K}{M_K} = \frac{(M_K - E_\nu)(E_\pi' + E_\mu') \pm |P_{yz}| (P_{\pi z}' + P_{\mu z}')}{(E_\pi' + E_\mu')^2 - (P_{\mu s}' + P_{\pi s}')^2}. \quad (8)$$

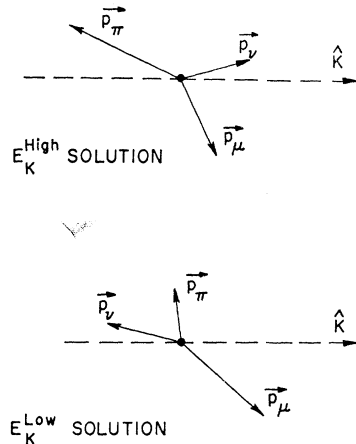


FIG. 5. Decay configurations for both kinematic solutions in the  $K_L^0$  rest frame for typical event.

$E_{\pi'}$  and  $E_{\mu'}$  are the laboratory energies of the pion and muon;  $P_{\pi z'}$  and  $P_{\mu z'}$  are the components of the pion and muon momenta along the  $K_L^0$  direction.  $E_{\nu}$  is the neutrino energy in the  $K_L^0$  rest frame;  $|P_{\nu z}|$  is the magnitude of the component of neutrino momentum along the  $K_L^0$  direction.

The transformation to the  $K_L^0$  rest frame is therefore not unique. Two possible sets of momentum vectors occur in the center-of-mass system. In Fig. 5, we display the two possible center-of-mass momentum configurations of a typical  $K_L^0$  decay in this experiment. For the solution of Eq. (8), where the  $K$  meson has the lower energy, the neutrino momentum  $\mathbf{p}$ , is directed backward relative to the  $K_L^0$  beam direction  $\hat{K}$ . The muon is typically directed forward because its laboratory momentum must be at least 540 MeV/c to pass through

the absorber. For the configuration, where the  $K$  meson has the higher energy, the neutrino is directed forward. The total neutrino momentum is the same for both configurations; all transverse components of momenta are the same for  $E_K^{\text{High}}$  as for  $E_K^{\text{Low}}$ . The pion and the muon are emitted less forward for  $E_K^{\text{High}}$  than for  $E_K^{\text{Low}}$ . The muon direction  $\hat{u}_L$  for the  $E_K^{\text{Low}}$  configuration differs only by about  $25^\circ$  from that of the  $E_K^{\text{High}}$  configuration. The sense of  $\hat{u}_T$  from Eq. (6) is opposite in the two cases. The direction  $\hat{u}_P$  from Eq. (7) differs markedly for the two configurations.

### B. Angular Distributions for Total Data

The angular distributions shown in Fig. 6 show the total data, 1602 events. These are events for which the positron track made an angle of at least  $30^\circ$  relative to the stopped muon track in the range spark chambers. Events that had a positron track within the forward  $30^\circ$  cone are not included. The longitudinal angular distribution in Fig. 6(a) shows a pronounced asymmetry; the transverse angular distribution in Fig. 6(b) shows no apparent asymmetry; the in-plane-perpendicular angular distribution in Fig. 6(c) shows a slight backward asymmetry. The distributions are not linear because of the anisotropic detection efficiency of the range spark chamber system.

For the data in Fig. 6, the kinematical quantities have been calculated in the  $K_L^0$  rest frame assuming the solution which resulted in the lower of the two possible values for the laboratory energy of the  $K_L^0$  meson (the  $E_K^{\text{Low}}$  solution). An analysis of the angular distributions of Fig. 6 was made by a Monte Carlo calculation described in Sec. IV F. In Secs. IV C–IV E, we describe a different method of analysis in which unambiguous events were selected from the data.

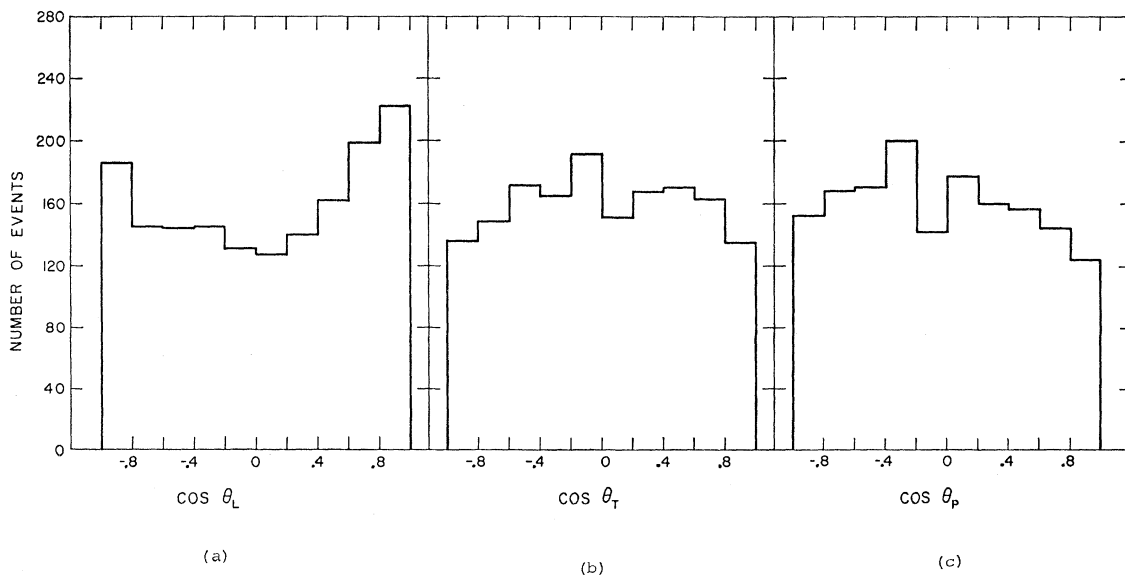


FIG. 6. The (a) longitudinal, (b) transverse, and (c) in-plane-perpendicular angular distributions of positrons for the total sample of 1602 events.

TABLE II. Selection of unambiguous subgroups of data.

Criteria	Number of events accepted as unambiguous		Number of events retained for further tests	Number of events rejected
	For in-plane components	For up-down components		
Initial data sample			1602	
1. $30^\circ \leq \theta_e \leq 150^\circ$			1459	143
2. $\gamma_{\text{High}} \geq 4.0$	347	347	1112	
3. $\cos\theta_L$ unambiguous $\cos\theta_T$ unambiguous $\cos\theta_P$ unambiguous	189	189	923	
4. $\cos\theta_L$ unambiguous $\cos\theta_P$ unambiguous	129		794	
5. $\cos\theta_L$ unambiguous $\cos\theta_T$ unambiguous		102		692
Totals accepted	665	638		

### C. Selection of Unambiguous Events

From the total sample of 1602 events, in which the  $\mu^+$  to  $e^+$  decay was observed, two unambiguous subgroups of events were selected (see Table II). The following procedure was used:

(1) Only those events were retained for which  $30^\circ \leq \theta_e \leq 150^\circ$ , where  $\theta_e$  is the angle between the positron track and the muon track in the range spark chambers. This cutoff cancels a bias in the longitudinal distribution [Fig. 6(a)] due to the cutoff  $30^\circ \leq \theta_e$  used in selecting events. Of the total of 1602 events, 1459 events satisfied this new criterion.

(2) A group of events was selected for which the higher-energy ( $E_K^{\text{High}}$ ) kinematic solution could be ruled out because of the  $K$ -meson energy spectrum and the  $K_{\mu 3}^0$  detection efficiency (Fig. 7). The  $K$ -meson energy spectrum was calculated from the results of a regeneration experiment ( $K_L^0 \rightarrow K_S^0 \rightarrow \pi^+\pi^-$ ) performed with a 3-in. copper regenerator in the same beam.<sup>8</sup> A constant regeneration amplitude was assumed in the calculation.<sup>9</sup> The detection efficiency was obtained from a Monte Carlo calculation.<sup>10</sup> As shown in Fig. 7, the  $K$ -meson energy spectrum decreased by a factor of 10 between  $E_K/M_K = 2.2$  and  $E_K/M_K = 4.0$ , while the detection efficiency varied by only  $\pm 10\%$  in that interval. For 347 events with  $E_K^{\text{High}}/M_K \geq 4.0$ , we used the  $E_K^{\text{Low}}$  solution; these events were selected from the 1459 which satisfied  $30^\circ \leq \theta_e \leq 150^\circ$ .

(3) The remaining 1112 events were tested to find those events for which both kinematic solutions gave the same polarization result. If both possible values of  $\cos\theta_L = \hat{u}_L \cdot \hat{e}$  fell in the same interval of the longitudinal angular distribution and if both values of  $\cos\theta_P = \hat{u}_P \cdot \hat{e}$  fell in the same interval of the in-plane-perpendicular angular distribution and if both possible values of  $\cos\theta_T = \hat{u}_T \cdot \hat{e}$  fell in the same interval of the up-down

angular distribution, the event was considered unambiguous. With the range of  $\cos\theta$  divided into six equal intervals, 189 of the 1112 events were found to be unambiguous; 923 events did not pass this test.

(4) The remaining 923 events were tested to find those events which were unambiguous only for the determination of the in-plane polarization. If both possible values of  $\cos\theta_L = \hat{u}_L \cdot \hat{e}$  fell in the same interval and if both possible values of  $\cos\theta_P = \hat{u}_P \cdot \hat{e}$  fell in the same interval, the event was used. Of the 923 events, 129 passed this test, giving a total of 665 events to be used for the analysis of the in-plane-perpendicular polarization. The angular distributions for these events are shown in Figs. 8(a) and 8(b).

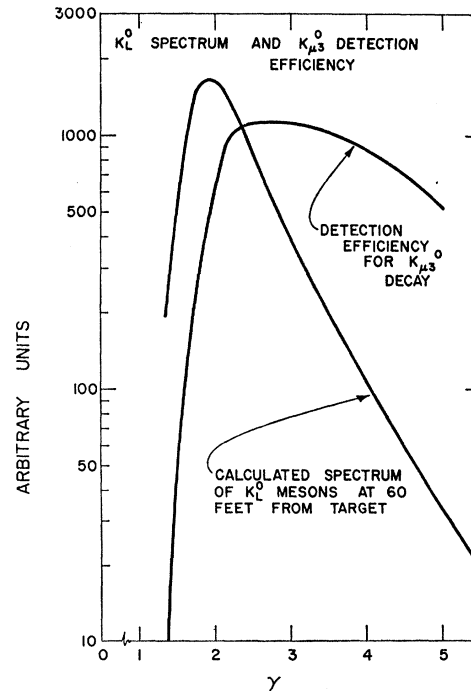


FIG. 7. Calculated energy spectrum of  $K_L^0$  mesons and relative detection efficiency for  $K_{\mu 3}^0$  decays plotted versus  $\gamma = E_K/M_K$ .

<sup>8</sup> R. E. Mischke, thesis, University of Illinois, 1966 (unpublished).

<sup>9</sup> The results of the present experiment are not very sensitive to the uncertainties in the  $K$ -meson energy spectrum.

<sup>10</sup> R. J. Abrams, thesis, University of Illinois, 1966 (unpublished).

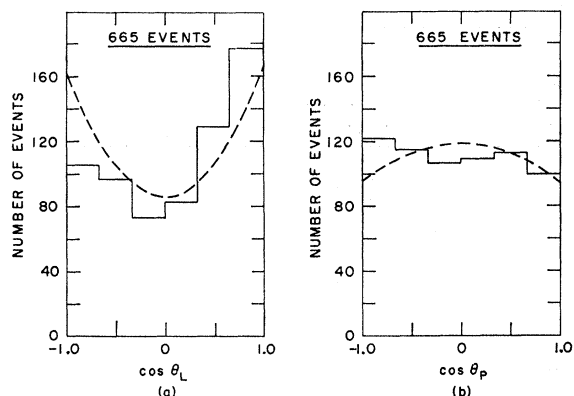


FIG. 8. Center-of-mass angular distributions for sample of 665 unambiguous events: (a) longitudinal, (b) in-plane-perpendicular. Dashed curves indicated expected shapes for an unpolarized sample.

(5) Similarly, if both possible values of  $\cos\theta_L$  fell in the same interval and both values of  $\cos\theta_T = \hat{u}_T \cdot \hat{e}$  fell in the same interval, the event was used for the analysis of the transverse polarization. Of the 794 events tested, 102 were found to satisfy the criterion, giving a total of 638 events for the analysis of the transverse polarization. The angular distributions are shown in Figs. 9(a) and 9(b).

#### D. Correction for Efficiencies

A correction was applied to the experimental angular distributions of Figs. 8 and 9 to account for

- (1) exclusion of events in which the angle between the positron track and the muon track was less than  $30^\circ$  or greater than  $150^\circ$ ,
- (2) selection of unambiguous events,
- (3) loss of steep positron tracks in the range spark chambers.

We obtained the relative detection efficiency for steep positron tracks from the observed angular distributions

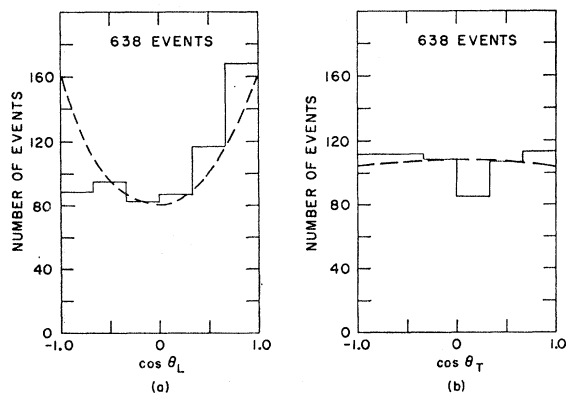


FIG. 9. Center-of-mass angular distributions for sample of 638 unambiguous events: (a) longitudinal, (b) transverse to the decay plane. Dashed curves indicate expected shapes for an unpolarized sample.

of electrons from stopped negative muons (see Fig. 10) from 340 events which fit  $K_L^0 \rightarrow \pi^+\mu^-\nu$ . Stopped negative muons are almost completely depolarized (84%) by orbital capture. In Fig. 10, events have been removed in which the electron angle relative to the stopping muon was greater than  $150^\circ$ . An empirical fit of the function

$$\eta(\cos\theta_{ez}) = 1 - A \exp(-B \cos^2\theta_{ez}) \quad (9)$$

resulted in  $A=0.95$ ,  $B=5.3$ , where  $\theta_{ez}$  is the angle between the electron track and the normal to the plates. In Fig. 10, the dashed curve shows the fitted function.

A Monte Carlo calculation was performed to compute the expected shapes of the center-of-mass positron angular distributions for our sample of  $K_{\mu 3}^0$  decays. For each measured  $K_{\mu 3}^0$  decay a group of simulated positrons was generated by the computer. The angular distribution of the simulated positrons was weighted according to Eq. (3) using an assumed polarization. Each positron momentum vector was rotated by an amount equal to the precession of the muon spin in the magnetic field. The laboratory angular distribution of positrons was weighted according to Eq. (9) to account for the loss of steep positron tracks in the range chambers. In addition, those candidates were not accepted for which the simulated positrons were emitted within  $30^\circ$  forward or backward relative to the muon-momentum vector in the laboratory. Ten simulated positrons were produced for each  $K_{\mu 3}^0$  of the actual data.

The selection of kinematically unambiguous Monte Carlo events was similar to the selections of unambigu-

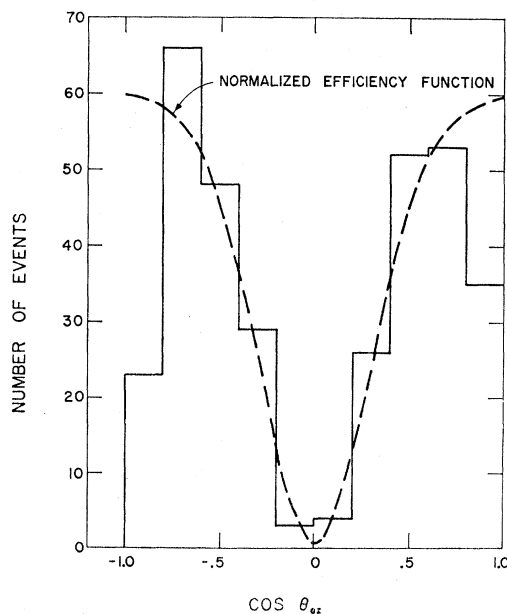


FIG. 10. Laboratory angular distribution of electrons from  $\mu^-$  events.  $\theta_{ez}$  is the angle between the electron direction and the normal to the plates of the range spark chambers.

ous real events. For each event in which  $E_K^{\text{High}}/M_K \geq 4$ , all Monte Carlo positrons were accepted for the  $E_K^{\text{Low}}$  solution. If  $E_K^{\text{High}}/M_K < 4$ , a comparison was made between the  $E_K^{\text{High}}$  values and the  $E_K^{\text{Low}}$  values of  $\hat{e} \cdot \hat{u}_L$ ,  $\hat{e} \cdot \hat{u}_T$ , and  $\hat{e} \cdot \hat{u}_P$  for each Monte Carlo positron. Only those Monte Carlo positrons were accepted for which both values of  $\hat{e} \cdot \hat{u}_L$ ,  $\hat{e} \cdot \hat{u}_T$ , or  $\hat{e} \cdot \hat{u}_P$  fell in the same interval of the angular distribution. To correct the data, the number of events in each bin in Figs. 8 and 9 was divided by the relative value from the dashed curves; the total number of events was then normalized to the original number. The corrected data are shown in Figs. 11 and 12.

### E. Least-Squares-Fit Results

We made least-squares fits to the data of Fig. 11 and Fig. 12 using linear functions of the form

$$dN_e/d(\cos\theta) = 1 + \alpha\bar{P} \cos\theta. \quad (10)$$

The results of the fits to the data of Fig. 11 are

$$\begin{aligned} \alpha\bar{P}_L &= 0.31 \pm 0.07, \\ \alpha\bar{P}_P &= -0.10 \pm 0.07. \end{aligned} \quad (11)$$

For the data of Fig. 12, the results are

$$\begin{aligned} \alpha\bar{P}_L &= 0.30 \pm 0.07, \\ \alpha\bar{P}_T &= -0.02 \pm 0.07. \end{aligned}$$

The longitudinal polarization  $\bar{P}_L$  is large, consistent with full polarization; the transverse polarization is consistent with zero; the in-plane-perpendicular polarization is small.

We define  $\varphi$  to be the angle in the decay plane between the polarization vector and the muon momentum; it is independent of the analyzing parameter  $\alpha$ . From the above results, we obtain

$$\tan\varphi = \frac{\alpha\bar{P}_P}{\alpha\bar{P}_L} = \frac{-0.10 \pm 0.07}{0.31 \pm 0.07} = -0.32 \pm 0.23. \quad (12)$$

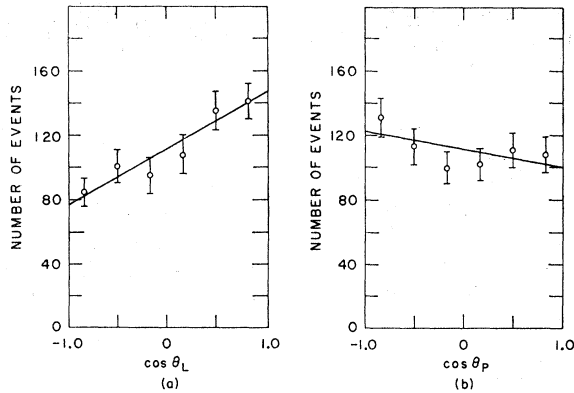


FIG. 11. Center-of-mass angular distributions for sample of 665 unambiguous events after correction for efficiencies: (a) longitudinal, (b) in-plane-perpendicular. Lines indicate least-squares-fit results.

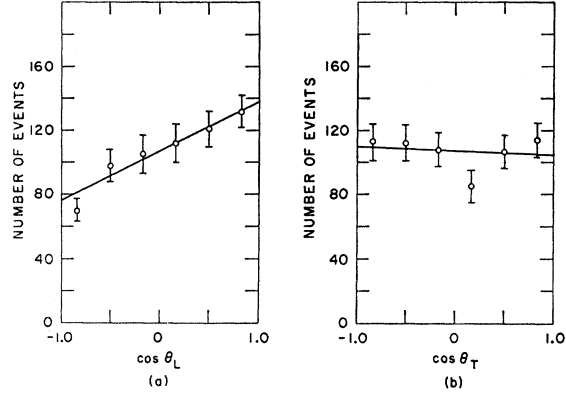


FIG. 12. Center-of-mass angular distributions for sample of 638 unambiguous events after correction for efficiencies: (a) longitudinal, (b) transverse to the decay plane. Lines indicate least-squares-fit results.

The theoretical relationship between  $\tan\varphi$  and  $\text{Re}\xi$ , integrated over the observed Dalitz plot density, is shown in Fig. 13. The experimental Dalitz plot is shown in Fig. 14. Since the transverse polarization was consistent with zero, we have assumed  $\text{Im}\xi = 0$  for Fig. 13. The value obtained for  $\tan\varphi$  corresponds to

$$\text{Re}\xi = -1.6 \pm 0.5, \quad \text{for } \text{Im}\xi = 0.$$

If we define  $\beta$  to be the angle between the polarization

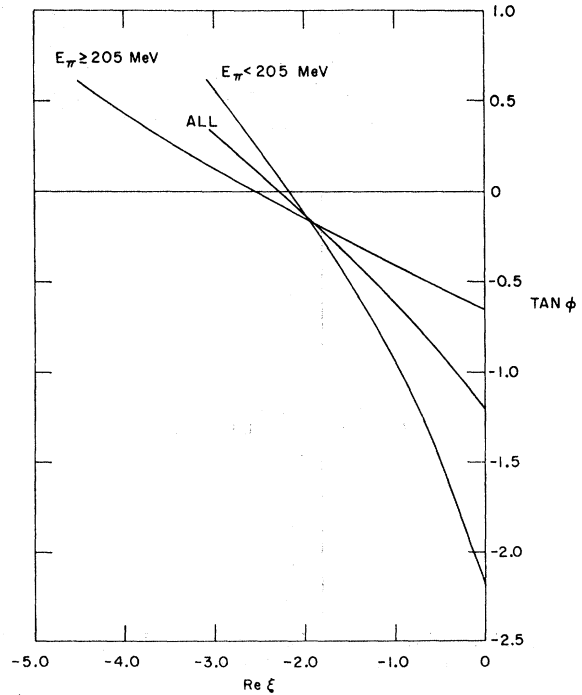


FIG. 13. Calculated relationships between  $\tan\varphi$  and  $\text{Re}\xi$  for  $\text{Im}\xi = 0$ . The curves are labeled to indicate integrals over the experimental Dalitz plot density taken for  $E_\pi \geq 205$  MeV, for  $E_\pi < 205$  MeV, and for the entire Dalitz plot.

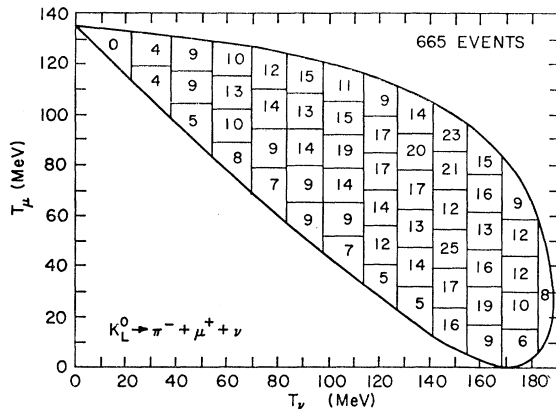


FIG. 14. Experimental Dalitz plot density corrected for the kinematic ambiguity.

vector and the decay plane, we have

$$\tan\beta = \frac{\alpha\bar{P}_T}{[(\alpha\bar{P}_L)^2 + (\alpha\bar{P}_P)^2]^{1/2}} = -0.08 \pm 0.23.$$

Similarly, we obtain a value  $\text{Im}\xi = -0.2 \pm 0.6$  for the curve in Fig. 15.

As a check on a possible energy dependence of the form factor ratio  $\text{Re}\xi$ , we have divided the data shown in Fig. 8 into two groups depending on the center-of-mass energy of the pion. Corrected angular distributions are shown in Fig. 16. There were 371 events with  $E_\pi < 205$  MeV and 294 events with  $E_\pi \geq 205$  MeV in the samples. From least-squares fits to the data of Fig. 16,  $\tan\varphi = -0.55 \pm 0.34$  for  $E_\pi < 205$  MeV and  $\tan\varphi = -0.03 \pm 0.35$  for  $E_\pi \geq 205$  MeV. From the curves in Fig. 13,  $\text{Re}\xi = -1.4 \pm 0.4$  for  $E_\pi < 205$  MeV<sup>11</sup> and

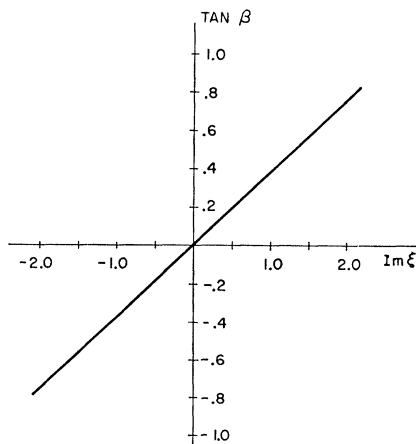


FIG. 15. Calculated relationship between  $\tan\beta$  and  $\text{Im}\xi$  integrated over the experimental Dalitz plot density.

<sup>11</sup> Although the experimental error in  $\tan\varphi$  is larger for the portion of the Dalitz plot with  $E_\pi < 205$  MeV than for the total data, it leads to an error in  $\xi$  of  $\pm 0.4$  for that part of the Dalitz distribution, while the total distribution has an error  $\pm 0.5$ . This arises from the greater slope for  $E_\pi < 205$  MeV in Fig. 13. If the

$\text{Re}\xi = -2.4 \pm 1.4$  for  $E_\pi \geq 205$  MeV. The size of the errors on  $\text{Re}\xi$ , particularly for  $E_\pi \geq 205$  MeV, does not allow a conclusion to be drawn about the energy dependence of the form factor ratio. As shown in Fig. 13, the polarization angle is much less sensitive to  $\text{Re}\xi$  for  $E_\pi \geq 205$  MeV than for  $E_\pi < 205$  MeV.

### F. Monte Carlo and $\chi^2$ Analysis

As a check on the least-squares analysis, a Monte Carlo analysis was made. It was possible to compare the Monte Carlo generated angular distributions directly with the angular distributions of Fig. 6; thus selection

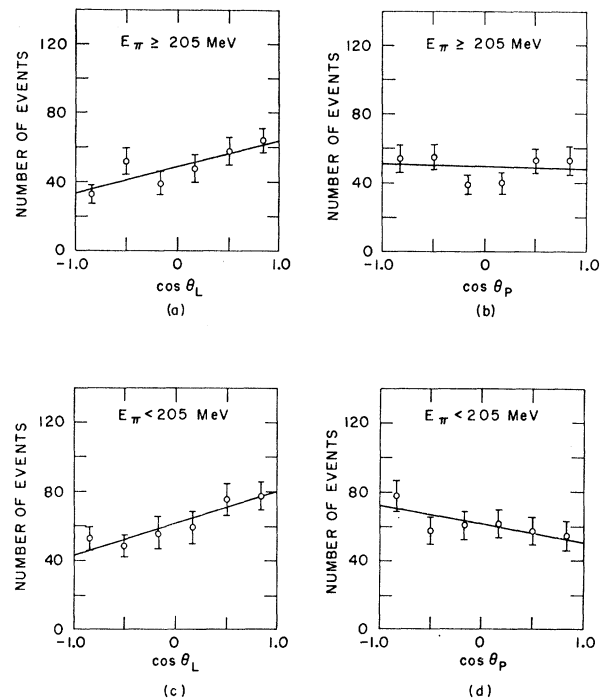


FIG. 16. Center-of-mass angular distributions for sample of 665 unambiguous events after correction for efficiencies: (a) longitudinal,  $E_\pi \geq 205$  MeV, (b) in-plane-perpendicular,  $E_\pi \geq 205$  MeV, (c) longitudinal,  $E_\pi < 205$  MeV, (d) in-plane-perpendicular,  $E_\pi < 205$  MeV.

of unambiguous events was unnecessary. The Monte Carlo calculation was parametrized such that a  $\chi^2$  analysis was made as a function of the form factor ratio  $\xi$ . Details of the method used to generate Monte Carlo events are given in Ref. 10. The  $K_L^0$  energies were picked at random from the beam energy spectrum (Fig. 7). The center-of-mass energies of the muon, pion, and neutrino were picked at random from the theoretical decay spectra. Random center-of-mass orientations

difference in the errors is significant, it may be arising from the simple treatment of the errors in the least-square analysis. A more elaborate treatment of the errors did not seem warranted in the light of the agreement with the results of the  $\chi^2$  analysis of Sec. IV F.

were picked. The polarization vector  $\hat{P}(\xi)$  was computed for each event according to Eq. (2). The angle between the positron and the polarization vector was chosen at random weighted according to Eq. (3). The laboratory angular distribution of the positrons was further weighted according to Eq. (9) to account for the detection efficiency for positrons in the range spark chambers.

For each Monte-Carlo-generated  $K_L^0$  decay the correct kinematic solution was known since the value of  $E_K$  was chosen in the calculation. Let  $E_K^{(1)}$  be the chosen value of the  $K_L^0$  energy, and  $E_K^{(2)}$  be the other (or incorrect) solution. If  $E_K^{(1)} \leq E_K^{(2)}$ , then  $E_K^{\text{Low}} = E_K^{(1)}$  and the three low-energy dot products were

$$\cos\theta_L = \hat{\epsilon}(\xi) \cdot \hat{u}_L^{(1)}, \quad (13)$$

$$\cos\theta_T = \hat{\epsilon}(\xi) \cdot \hat{u}_T^{(1)}, \quad (14)$$

$$\cos\theta_P = \hat{\epsilon}(\xi) \cdot \hat{u}_P^{(1)}, \quad (15)$$

where  $\hat{u}_L^{(1)}$  denotes a unit vector along the muon momentum, computed from the  $E_K^{(1)}$  kinematic solution, etc. If, on the other hand,  $E_K^{(1)} > E_K^{(2)}$ , then  $E_K^{\text{Low}} = E_K^{(2)}$  and the three low-energy dot products were computed as

$$\cos\theta_L = \hat{\epsilon}(\xi) \cdot \hat{u}_L^{(2)}, \quad (16)$$

$$\cos\theta_T = \hat{\epsilon}(\xi) \cdot \hat{u}_T^{(2)}, \quad (17)$$

$$\cos\theta_P = \hat{\epsilon}(\xi) \cdot \hat{u}_P^{(2)}. \quad (18)$$

In this way, the  $E_K^{\text{Low}}$  angular distributions were obtained for each value of  $\xi$  tested. The  $E_K^{\text{Low}}$  angular distributions obtained were thus directly comparable with the data of Fig. 6.

A Monte Carlo sample of 4000 detectable  $K_L^0$  decays was generated; three detectable positrons were generated for each value of the form factor ratio  $\xi$  for every

$K_L^0$  decay. The  $E_K^{\text{Low}}$  Monte Carlo angular distributions were normalized to the total number of data events, then smoothed using least-squares-fitted parabolas. The smoothed angular distributions for each value of  $\xi$  were compared to the  $E_K^{\text{Low}}$  distributions for the total data (1602 events in Fig. 6). The following  $\chi^2$  functions were used:

$$\chi_L^2(\xi) = \sum_{j=1}^{10} \frac{[T_{jL}(\xi) - D_{jL}]^2}{T_{jL}(\xi)}, \quad (19)$$

$$\chi_T^2(\xi) = \sum_{j=1}^{10} \frac{[T_{jT}(\xi) - D_{jT}]^2}{T_{jT}(\xi)}, \quad (20)$$

$$\chi_P^2(\xi) = \sum_{j=1}^{10} \frac{[T_{jP}(\xi) - D_{jP}]^2}{T_{jP}(\xi)}, \quad (21)$$

where the symbols  $D_{jL}$  and  $T_{jL}$  represent the numbers of events in the  $j$ th bin of the longitudinal angular distributions for the data and for the smoothed Monte Carlo sample, respectively. The subscripts  $T$  and  $P$  denote the transverse and in-plane-perpendicular, respectively. The angular distributions were divided into 10 equal bins.

The results of the  $\chi^2$  tests are shown in Table III. The values obtained for  $\chi_L^2$ ,  $\chi_T^2$ , and  $\chi_P^2$  are displayed in matrices as functions of  $\text{Re}\xi$  and  $\text{Im}\xi$ . Examination of Table III shows that  $\chi_T^2$  is insensitive to  $\text{Re}\xi$ , but that  $\chi_T^2$  has a minimum at  $\text{Im}\xi = 0$  for nearly all values of  $\text{Re}\xi$ .  $\chi_P^2$  is insensitive to  $\text{Im}\xi$ , but negative values of  $\text{Re}\xi$  are favored over positive values. The  $\chi_L^2$  plot has a broad minimum from  $-2.5 < \text{Re}\xi < -1.0$ . The sum  $\chi_L^2 + \chi_P^2 + \chi_T^2$  has a minimum value of 24.83 at  $\text{Re}\xi = -1.8$ ,  $\text{Im}\xi = 0$ .

Because  $\chi_T^2$  was insensitive to  $\text{Re}\xi$  we have combined  $\chi_L^2$  and  $\chi_P^2$ , with  $\text{Im}\xi = 0$ , to determine  $\text{Re}\xi$ . In Fig. 17,

TABLE III. Results of  $\chi^2$  calculations.

	$\text{Im}\xi \backslash \text{Re}\xi$								
		-3.0	-2.4	-1.8	-1.2	-0.6	0.0	0.6	1.2
$\chi_L^2$ , longitudinal	2	12.46	14.03	14.07	13.11	14.54	19.49	21.98	24.41
	1	9.30	6.82	8.23	8.52	9.90	13.38	21.11	20.61
	0	9.97	5.83	5.39	5.82	8.73	9.58	12.07	20.21
	-1	8.45	8.09	9.24	5.90	8.89	11.53	16.88	24.47
	-2	21.20	16.86	14.36	11.63	12.64	22.57	20.09	27.01
$\chi_T^2$ , transverse	2	23.09	23.22	20.56	19.31	23.00	12.14	11.35	13.32
	1	10.63	11.32	12.88	10.98	10.08	11.27	9.76	10.02
	0	11.62	8.73	8.74	7.57	11.76	9.12	7.69	6.94
	-1	17.00	16.61	15.93	14.18	12.31	11.67	10.12	9.90
	-2	22.72	21.34	25.19	24.48	21.57	19.46	13.60	10.95
$\chi_P^2$ , in-plane-perpendicular	2	14.61	11.46	10.83	14.56	16.15	19.90	22.53	25.61
	1	15.81	12.60	10.66	11.53	19.12	23.56	24.30	25.63
	0	14.64	11.66	10.69	12.20	18.20	24.19	25.42	31.62
	-1	15.99	12.29	10.70	13.63	15.93	22.18	27.59	29.13
	-2	13.37	11.68	11.56	13.78	14.58	22.38	24.61	24.32
$\chi_L^2 + \chi_T^2 + \chi_P^2$	2	50.15	48.71	45.46	46.98	53.69	51.53	55.87	63.34
	1	35.73	30.75	31.77	31.03	39.09	48.21	55.18	56.25
	0	36.23	26.21	24.83	25.60	38.69	42.89	45.18	58.76
	-1	41.44	37.00	35.87	33.71	37.13	45.39	54.59	65.50
	-2	57.29	49.88	51.10	49.90	48.79	64.42	58.29	62.28

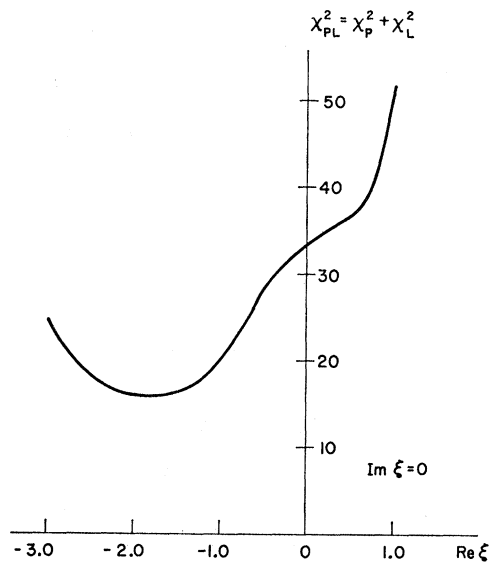


FIG. 17.  $\chi^2$  versus  $\text{Re } \xi$  for in-plane components of polarization.

$\chi_{PL}^2$  is plotted versus  $\text{Re } \xi$ , where

$$\chi_{PL}^2 = \chi_P^2 + \chi_L^2. \quad (22)$$

The minimum value,  $\chi_{PL}^2 = 16.1$ , occurs for  $\text{Re } \xi = -1.8 \pm 0.5$ . The minimum value of  $\chi_{PL}^2$  corresponds to a probability of 52% for 17 degrees of freedom, a reasonable fit. The errors correspond to the points at which  $\chi_{PL}^2$  increases by one unit. This value of  $\text{Re } \xi$  is consistent with the value  $\text{Re } \xi = -1.6 \pm 0.5$  obtained from least-squares fits to the corrected unambiguous data as presented in the previous sections.

We have used  $\chi_T^2$  at  $\text{Re } \xi = -1.8$  to determine the best value of  $\text{Im } \xi$  (Fig. 18). The minimum value,

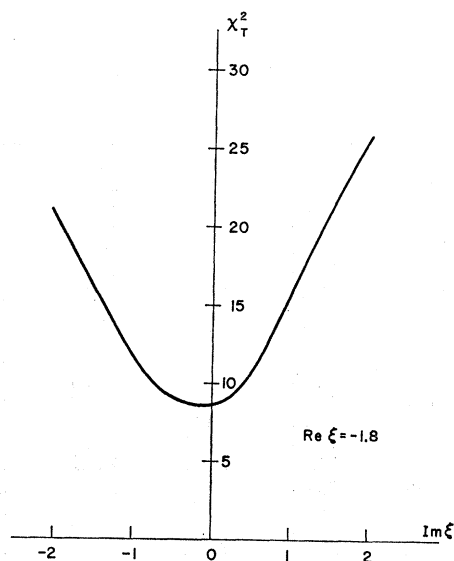


FIG. 18.  $\chi^2$  versus  $\text{Im } \xi$  for transverse polarization.

$\chi_T^2 = 8.7$ , occurs for  $\text{Im } \xi = 0.1 \pm 0.5$ . The minimum value of  $\chi_T^2$  corresponds to a probability of 36% for 8 degrees of freedom. This result is consistent with the result  $\text{Im } \xi = -0.2 \pm 0.6$  obtained from least-squares fits to the corrected unambiguous data.

## V. CONCLUSIONS

The magnitude of the polarization of the muon from  $K_{\mu 3}^0$  decay was found to be consistent with the theoretically expected complete polarization. From the direction of the polarization we found an average value of  $\text{Re } \xi = -1.6 \pm 0.5$  for the form factor ratio. Our result is in agreement with the result  $\text{Re } \xi = -1.2 \pm 0.5$  by Auerbach *et al.*,<sup>3</sup> from a measurement of the in-plane-perpendicular component of the muon polarization in  $K_{\mu 3}^0$  decay. Our result is in reasonable agreement with recent measurements of the muon polarization in  $K_{\mu 3}^+$  by Cutts *et al.*,<sup>12</sup> and in  $K_{\mu 3}^0$  by Helland *et al.*,<sup>13</sup> who reported values of  $\text{Re } \xi = -0.95 \pm 0.3$  and  $\text{Re } \xi = -1.75_{-0.2}^{+0.5}$ , respectively. These results are consistent with the  $\Delta I = \frac{1}{2}$  rule which predicts that the  $K_{\mu 3}^+$  and  $K_{\mu 3}^0$  form factor ratios be equal. Our result  $\text{Im } \xi = -0.2 \pm 0.6$  derived from the transverse polarization is consistent with zero in agreement with time-reversal invariance.

As a check for possible energy dependence of the form factor ratio, we analyzed separately the polarization for two different ranges of pion energy (or four-momentum transfer). For pion energy  $E_\pi < 205$  MeV we found  $\text{Re } \xi = -1.4 \pm 0.4$ ; for pion energy  $E_\pi \geq 205$  MeV we found  $\text{Re } \xi = -2.4 \pm 1.4$ . The statistical errors, particularly for  $E_\pi \geq 205$  MeV, are too large for a conclusion to be drawn about the energy dependence of the form factor ratio. The intrinsic lack of sensitivity for  $E_\pi \geq 205$  MeV makes it more difficult to measure  $\xi$  precisely in that part of the Dalitz plot.

There is a need for more precise measurements of the polarization over the whole Dalitz plot to determine the energy dependence of the form factors. The intrinsic lack of sensitivity for the higher pion energy region will make it more difficult to obtain the desired precision.

It is to be pointed out that although all the values of  $\text{Re } \xi$  obtained from the polarization measurements of both  $K_L^0$  and  $K^+$  are in agreement, they seriously disagree with the value of  $\text{Re } \xi$  obtained from a measurement of a branching ratio of  $K_{\mu 3}^0/K_{e 3}^0$ .<sup>14</sup> Attempts by Auerbach *et al.*<sup>4</sup> to resolve this discrepancy by employing form factors that have large energy dependencies have not been very satisfactory. Therefore, it is obviously very important that improved measurements

<sup>12</sup> D. Cutts, R. Stiening, C. Wiegand, and M. Deutsch, Phys. Rev. Letters 20, 955 (1968).

<sup>13</sup> J. A. Helland, M. J. Longo, and K. K. Young, Phys. Rev. Letters 21, 257 (1968).

<sup>14</sup> L. B. Auerbach, J. Dobbs, A. K. Mann, W. K. McFarlane, D. H. White, R. Cester, P. T. Eschtruth, G. K. O'Neill, and D. Yount, Phys. Rev. 155, 1505 (1967).

of the branching ratio as well as of the polarization be made.

The comparison of the value of  $Re\xi$  obtained from the branching ratio with  $Re\xi$  obtained from a measurement of  $K_{\mu 3}$  alone is based on the assumption of  $\mu$ - $e$  universality. Lee and Wu (Ref. 5, p. 491), using earlier data which were not as precise, drew the conclusion that there was evidence for  $\mu$ - $e$  universality in the  $K$  decays. Until one understands the present discrepancy, the conclusion that there is  $\mu$ - $e$  universality in  $K$  decays is not valid.

## ACKNOWLEDGMENTS

We wish to acknowledge the advice and assistance of Dr. D. W. Carpenter, particularly during the analysis of this experiment. We would like to thank the staff of the Argonne Zero Gradient Synchrotron for their cooperation. We are very indebted to C. Smock, L. Seward, H. Barton, P. Mantsch, and E. Harris for their help in the construction of the apparatus and in the running of the experiment. We are grateful to Mrs. P. Martin for her careful supervision of the scanning and measuring.

## Relativistic Energy Loss by Ionization in Nuclear Emulsions

F. J. CONGEL\* AND P. J. McNULTY

*Physics Department, Clarkson College of Technology, Potsdam, New York 13676*

(Received 1 July 1968)

The variation in grain density in the tracks of 5-, 8-, 12-, and 24-GeV/ $c$  protons and 5-GeV/ $c$  pions has been investigated as a function of velocity in the same plate of an Ilford K-5 nuclear emulsion. About 80 000 blobs were counted for each beam. The pion-to-proton ratio of grain densities at 5 GeV/ $c$  is  $1.114 \pm 0.006$ . The results are in agreement with the Sternheimer formula using a mean ionization potential for AgBr of 434 eV and a cutoff energy  $T_0$  of 2-5 keV. Comparison of these data with an earlier experiment in a G-5 emulsion shows no dependence of the rate of the relativistic rise in grain density on type of emulsion. The combined data from the two experiments are in excellent agreement with Sternheimer's formula with  $I=434$  eV and  $T_0=5$  keV with no correction due to secondary ionization. A correction for secondary ionization corresponding to a 10% contribution due to secondary ionization at minimum ionization gives excellent agreement with  $I=434$  eV and  $T_0=2$  keV.

## I. INTRODUCTION

THERE have been many attempts to measure the relativistic rise of the grain density in nuclear emulsions, and much evidence<sup>1-14</sup> has been accumulated to support a proportionality between the grain density and the restricted energy loss given by the Sternheimer

formula.<sup>16-19</sup> In comparing their data with the Sternheimer formula, the parameters  $I$  (mean ionization potential of emulsion atoms) and  $T_0$  (allowed energy transferred in individual collisions) have been varied by experimenters to obtain a best fit yielding, however, a wide fluctuation in the values of both constants. In most of the previous experiments, the relativistic rise was calculated from the ratio of grain density measurements at large values of  $\gamma$  [ $\gamma = (1 - v^2/c^2)^{-1/2} > 200$ ] and at minimum ionization ( $3 \leq \gamma \leq 4$ ). Objections can be raised to this method of measurement, however. Theoretical and experimental studies by Patrick and Barkas<sup>9</sup> on the effect of secondary grain densities (i.e., due to  $\delta$  rays) would seem to indicate that a shift of as much as 6% might be expected in the ratio of the plateau to minimum grain densities from that predicted by Sternheimer's formula, while the second-order radiative correction predicted by Tsytovtich<sup>20</sup> would introduce another correction of 4-5% in the asymptotic region.

\* National Science Foundation Trainee. Present address: Argonne National Laboratory, Argonne, Ill.

<sup>1</sup> E. Pickup and L. Voyvodic, Phys. Rev. **80**, 89 (1950).

<sup>2</sup> M. M. Shapiro and B. Stiller, Phys. Rev. **87**, 682 (1952).

<sup>3</sup> R. Michaelis and C. Violet, Phys. Rev. **90**, 723 (1953).

<sup>4</sup> A. Morrish, Phys. Rev. **91**, 423 (1953).

<sup>5</sup> J. Fleming and J. Lord, Phys. Rev. **92**, 511 (1953).

<sup>6</sup> B. Stiller and M. M. Shapiro, Phys. Rev. **92**, 735 (1953).

<sup>7</sup> G. Alexander and R. Johnston, Nuovo Cimento **5**, 363 (1957).

<sup>8</sup> B. Jongejans, Nuovo Cimento **26**, 626 (1960).

<sup>9</sup> J. Patrick and W. Barkas, Nuovo Cimento Suppl. **23**, 1 (1962).

<sup>10</sup> B. Stiller, in *Proceedings of the Fourth International Conference on Corpuscular Photography*, edited by H. Freiser and G. Heiman (Munich, 1963), p. 542.

<sup>11</sup> F. R. Buskirk, J. N. Dyer, H. D. Hanson, R. Seng, and R. H. Weidman, CERN Report No. 65-4 (unpublished).

<sup>12</sup> A. J. Herz and B. Stiller, in *Proceedings of the Fifth International Conference on Corpuscular Photography*, edited by E. Dahl-Jensen (CERN, Geneva, 1965).

<sup>13</sup> Z. V. Anzon, A. Vinitskii, Z. S. Takaibaev, I. Y. Chasnikov, and T. I. Shakova, Zh. Eksperim. i Teor. Fiz. **47**, 2051 (1964) [English transl.: Soviet Phys.—JETP **20**, 1378 (1965)].

<sup>14</sup> C. A. Nicoletta, P. J. McNulty, and P. L. Jain, Phys. Rev. **164**, 1693 (1967).

<sup>15</sup> R. M. Sternheimer, Phys. Rev. **88**, 851 (1952).

<sup>16</sup> R. M. Sternheimer, Phys. Rev. **91**, 256 (1953).

<sup>17</sup> R. M. Sternheimer, Phys. Rev. **103**, 511 (1956).

<sup>18</sup> R. M. Sternheimer, Phys. Rev. **145**, 247 (1966).

<sup>19</sup> R. M. Sternheimer, Phys. Rev. **164**, 349 (1967).

<sup>20</sup> V. N. Tsytovtich, Dokl. Akad. Nauk SSSR **144**, 310 (1962) [English transl.: Soviet Phys.—Doklady **7**, 411 (1962)].